A Quantification of the Performance Loss of Power Averaging in Airborne Wind Energy Farms

E.C. Malz[1] , M. Zanon[2] , S. Gros[1]

***Abstract*— Airborne wind energy (AWE) is a promising source of renewable energy, with a potential of offering great and reliable energy yields. However, in addition to the usual power intermittency of renewable source of energies, AWE systems have a large and periodic fluctuation of their power output, and even consume power at certain phases of their orbit in some modes of power generation. These fluctuations may become a significant obstacle to a large-scale deployment of AWE systems in the power grid. For a large AWE farm, these fluctuations can be mitigated by power averaging, at the expense of fixing the AWE systems orbit times. This requirement removes the possibility for individual AWE systems within a wind farm to optimize their orbit time for their specific, local wind conditions, entailing a loss of performance. In order to assess the viability of mitigating the power fluctuation by power averaging at the wind farm level, this paper quantifies the loss of performance it yields.**

I. Introduction

Airborne Wind Energy (AWE) systems harvest wind energy by means of tethered wings flying autonomously in a crosswind fashion. By accessing the better and more stable wind conditions present at high altitudes, the AWE technology promises a more reliable wind power generation than the classical wind-energy industry. Because AWE does not require a tower or blades, it can be based on light-weight constructions, hence reducing the material costs. The wings are connected directly to a ground station by a tether. By transmitting the thrust forces directly to the ground, the need for building heavy and expensive foundations is reduced [1].

Two major AWE concepts are considered by the industry: pumping and drag mode. Drag mode AWE systems are based on on-board power generation and rigid-wing flying crosswind circles or lemniscates at high velocities. The power is generated by on-board turbine(s) operating at high wind velocities and transferred to the ground station via the tether [2].

Pumping mode AWE systems can use both rigid and soft wings. The power is generated by exploiting the large lift forces developed by the kite during fast cross-wind flight. These forces are used in order to reel out the tether from a winch attached to a generator. The power generation has to be regularly interrupted to retract the wing and the tether. This retraction phase typically consumes a fraction of the power produced during the reel-out phase [3, 4].

[1] Department of Electrical Engineering, Chalmers University of Technology, 412 96 Göteborg, Sweden {elenama ,grosse} @chalmers.se

[2] IMT School for Advanced Studies Lucca, 55100 Lucca, Italy mario.zanon@imtlucca.it

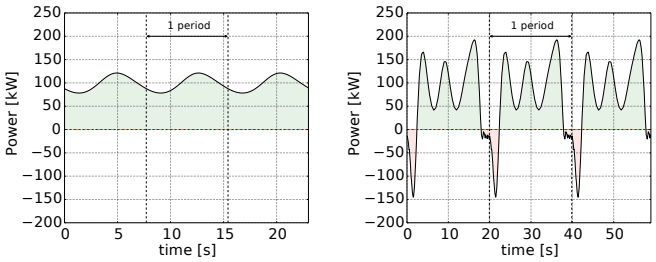

(a) Drag mode (b) Pumping mode

Fig. 1: Characteristic power generation for a wing in either drag mode or pumping mode, generating an average power output of 48,4 kW and 56.74 kW, respectively.

By its nature, the power generated by AWE systems is fluctuating. Even for AWE systems in drag mode, which do not go through a retraction phase, the power fluctuates periodically during one orbit. This fluctuation is caused by gravity and the wind shear, forcing the wing into a dissymmetric flight pattern. AWE systems in pumping mode have an even larger power fluctuation because the power generation is cyclically interrupted for the retraction phase. Fig.1 illustrates a simulated power generation profile of drag mode and pumping mode respectively. The severe intermittency due to the retraction phase in the pumping mode can be observed in Fig. 1b.

A successful commercialisation and integration to the power grid implies the installation of AWE farms. Ampyx Power, as an example, is planning to repower the current generation offshore wind parks with AWE [5]. Fluctuations of the power generation in a plant have to be compensated by other power plants in order to balance the power demand and production, and to maintain the grid frequency [6]. Modern power grids are used to deal with fluctuations arising from well-established sources of renewable energies. However, the power profiles of AWE systems, especially pumping mode, are rather unusual compared to other sources of renewable energy, and the future impact of AWE on the power grid is unclear.

AWE farms at the multi mega-watt (MMW) scale may reach a high level of penetration in future power systems, hence the issue of grid integration needs thorough investigations. In order to ensure the power grid stability, all connected power generation units have to follow certain grid codes [7]. No grid requirement dedicated to AWE systems has been formulated yet, but power outputs fluctuating significantly and cyclically are likely to be a serious obstacle

to a large-scale integration of AWE systems. Future grid codes are therefore expected to constrain AWE farms to deliver a sufficiently smooth power output.

A tentative solution for AWE farms to deliver a less fluctuating power consists in shifting the phase of the cyclic operation of the different wings within the AWE farm in order to balance the power fluctuations within the AWE farm itself. E.g. for an AWE farm with pumping mode systems, the periodical retraction phase of the various wings can be shifted such that the power required for the retraction is provided by the neighbouring AWE systems in the same farm. This approach is simulated and illustrated in Fig. 2 where an example of shifting can be observed. In Fig. 2a four AWE systems (grey) in pumping mode are controlled to be phase-shifted by a quarter of their orbit time. This phase-shifting adds up to a continuous total power (green), eliminating the consumption periods. In comparison, Fig. 2b displays the same individual profiles without a phase-shift, adding up to a much higher power variation than with shifting. The power averaging effect introduced by shifted operations tends to increase with the number of AWE systems present in an AWE farm.

In an AWE farm, the individual systems encounter slightly different wind conditions. Local wind variations translate into change in speed of the individual wings resulting in variations of the orbit time. The phase-shifted operation of the individual wings in an AWE farm is then gradually and non-uniformly modified over time. Because the wind variations are stochastic, the phase-shifts of the individual AWE systems in an AWE farm also become stochastic. Additionally, the power output of a classical wind farm is influenced by wake effects to a great extent [8]. However, the effect on AWE systems is not known yet and therefore not taken into account in this paper. In the future, wake models, more realistic wind profiles and accurate airfoil models will be implemented.

In a large wind farm, the combination of a great number of power profiles having stochastic phase-shifts is expected to deliver a fairly constant total power output with a relatively high probability. However, it can also deliver dramatic power variations with a non-negligible probability when the combination of the individual phases end up in a poor configuration. Because the phases are evolving slowly, such a situation could last for several minutes. The industry is considering addressing this problem by controlling the phase-shift of the individual AWE systems such that a poor combination of phases cannot occur. Such a scenario requires that all systems in the farm follow the same trajectory and orbit time, and reject the local disturbances on the phases via feedback control. An alternative to this approach would consider the joint optimization of the whole wind farm for power generation vs. power smoothing. This approach is, however, considered prohibitively complex to deploy and thus the first approach, the phase-shift control will be studied.

The economic viability of AWE will require the AWE systems to be operated optimally. Individual AWE systems

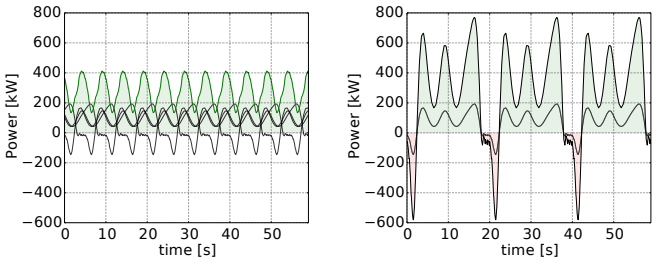

(a) Power summation (green) of shifted trajectories (grey)

(b) Power summation of synchronised trajectories

Fig. 2: Possible summation of power generation profiles of four systems with phase-shifted (left) and synchronised (right) trajectories.

ought to continuously adjust their trajectories to the wind condition in order to maximize their average power output. Early results in AWE system control show some promising approaches to achieve that [9, 10]. Unfortunately, the power optimisation of individual AWE systems is in conflict with phase control. Indeed, the optimal operation of a system typically requires adjustments in the wing trajectory and therefore in its orbit time. The system cannot be both operated optimally and have a fixed phase. In this study, we investigate this conflict, and quantify the loss of performance that is expected from applying phase control in an AWE farm. This paper compares the performance of an AWE farm where the orbit times are fixed and optimum for the average wind speed of the wind farm vs. an AWE farm where the individual AWE systems are optimum with a free orbit time. In the following, the two cases will be referred to as *fixed* and *free* time operation. Quantifying the power loss for a fixed-time operation is crucial for the AWE industry and might guide the future control designs of AWE farms.

The paper is structured as follows. In Section II the power optimisation of a single system and its formulation as a parametric optimal control problem is presented. The optimal cost at the solution is approximated as a second-order Taylor expansion in order to perform sensitivity studies with respect to the wind parameters. This will be used in Section II-B to compute the expected power of an AWE farm in the fixed and free-time mode. The results are presented in Section III where the loss in power due to a fixed orbit time is investigated for both drag mode and pump mode systems. The power loss is quantified for different sizes, as a function of the variance of the local wind variations and for different average wind speeds. Finally, in IV conclusions are drawn.

II. Method

The wind profile for an individual AWE system in the farm is described using the standard logarithmic wind profile [11]:

$$w = w_0 \left(\frac{h}{h_0}\right)^{z_0} = (\overline{w}_0 + \Delta w_0)\left(\frac{h}{h_0}\right)^{\overline{z}_0 + \Delta z_0} \tag{1}$$

where w is the wind at the height h, $w_0 \in \mathbb{R}$ denotes the base wind at a the reference height h_0 and $z_0 \in \mathbb{R}$ is the

aerodynamic roughness length. Note that there exists more realistic models, but (1) is used here for simplicity.

The local variation in wind speeds Δw_0 within a farm is assumed to be zero-mean gaussian distributed, with standard deviation σ_{w_0}, i.e. individual systems in a farm have a base wind $\overline{w}_0 + \Delta w_0$, where $\Delta w_0 \sim \mathcal{N}(0, \sigma_{w_0}^2)$ and $\overline{w}_0$ is the average wind speed on the wind farm. The roughness variation Δz_0 is also assumed to be zero-mean gaussian distributed, i.e. $\mathcal{N}(0, \sigma_{z_0}^2)$, and models a non-uniform wind shear within a farm. The optimal operation and performance of an individual AWE system within a farm then depends on the average base parameters $\overline{p} = (\overline{w}_0, \overline{z}_0)$ and their variations $\Delta p = (\Delta w_0, \Delta z_0)$.

A. Power optimisation problem

The optimal performance $\Phi^\star$ of a single AWE system is computed by solving the periodic optimal control problem (OCP)

$$\begin{aligned}
\Phi^\star(p,T) = \min_{x,z,u} \quad & \Phi(x,z,u,p,T) && \text{(2a)}\\
\text{s.t.} \quad & F(\dot{x},x,z,u,p,T) = 0, && \text{(2b)}\\
& c(x(0),x(T)) = 0, && \text{(2c)}\\
& h(x,z,u,p,T) \leq 0, && \text{(2d)}
\end{aligned}$$

where F is the model of an individual AWE system in the form of an implicit Differential-Algebraic Equation (DAE). x, z collect its differential and algebraic states respectively, and u the control inputs. Parameter T denotes the orbit time. Constraint (2c) enforces periodicity of the trajectories and (2d) gathers the actuator and operational limitations of the AWE system. The model F describes the wing in minimal coordinates as a point mass model with 6 DOF without any tether dynamics. Further, it contains an aerodynamic model, i.e. aerodynamic forces and moments acting on the wing depending on the current position and wind conditions. (2b) - (2d) depend on the considered system and the level of accuracy. A detailed description of the model used in this paper can be found in [10, 12].

The cost function Φ is given by the sum of the average power $P(x,p,T)$ during one orbit and a small quadratic regularisation term $\ell_{\text{Reg}}(u)$ on the control inputs u [10], i.e.:

$$\Phi(x,z,u,p,T) = \quad -\frac{1}{T}\int_0^T P(x,p,T) + \ell_{\text{Reg}}(u)\,\mathrm{d}t. \quad (3)$$

In practice, it can be noted that the regularisation term in the performance Φ is negligibly small, hence the performance is comparable with the generated average power of the AWE system. We need to underline here that the optimal trajectory for an individual AWE system disregards the problem of respecting an assigned phase and freely optimizes the orbit time T for the given wind conditions p, resulting in the performance:

$$\Phi^\star_{\text{free}}(p) = \min_T \Phi^\star(p,T) \leq \Phi^\star(p,T). \quad (4)$$

The difference $\Phi^\star(p,T) - \Phi^\star_{\text{free}}(p) \geq 0$ is then the performance loss incurred by assigning the orbit time T of the AWE system independently of the wind condition.

B. Wind parameter distribution and expected performance

A possible approach to investigate the effect of stochastic wind changes in the AWE farm is to extensively sample the distribution of the wind parameters, solving the OCP (2) for each sample. In this paper, we propose to use a more efficient approach based on the parametric sensitivity of the NLP underlying OCP (2). We detail this approach next.

The expected change in performance $\Phi^\star$ under the normal distributed wind parameter variation Δp and a change in orbit time T is given by $\mathbb{E}_{\Delta p}\left[\Delta\Phi^\star\right]$ where

$$\Delta\Phi^\star = \Phi^\star\left(\overline{p}+\Delta p, \overline{T}+\Delta T\right) - \Phi^\star\left(\overline{p},\overline{T}\right) \quad (5)$$

and $\overline{T} = \arg\min_T \Phi^\star(\overline{p},T)$, the optimal orbit time under the conditions $\bar{p}$. In the following, we use the second-order Taylor expansion:

$$\begin{aligned}
\Delta\Phi^\star = \quad & \nabla_p\Phi^{\star\top}\Delta p + \tfrac{1}{2}\Delta p^\top\nabla_p^2\Phi^\star\Delta p + \tfrac{1}{2}\Delta T^\top\nabla_T^2\Phi^\star\Delta T\\
& + \Delta p^\top\nabla_{pT}^2\Phi^\star\Delta T + \mathcal{O}\left(\|\Delta p,\Delta T\|^3\right), \quad (6)
\end{aligned}$$

where all terms are evaluated at $\overline{p},\overline{T}$. Using $\mathcal{L}$ as the Lagrange function of OCP (2), we observe that $\nabla_T\Phi^\star = \nabla_T\mathcal{L}^\star = 0$ since $\overline{T}$ is optimum for $\Phi^\star\left(\overline{p},\overline{T}\right)$ [13]. The impact of a change in the orbit time ΔT on $\Phi^\star$ is therefore of second order. The terms of order higher than 2 are neglected so that the expected power is approximated as:

$$\begin{aligned}
\mathbb{E}_{\Delta p}\left[\Delta\Phi^\star\right] \approx \quad & \mathbb{E}_{\Delta p}\Big[\nabla_p\Phi^{\star\top}\Delta p + \frac{1}{2}\Delta p^\top\nabla_p^2\Phi^\star\Delta p\\
& + \frac{1}{2}\Delta T^\top\nabla_T^2\Phi^\star\Delta T + \Delta p^\top\nabla_{pT}^2\Phi^\star\Delta T\Big]. \quad (7)
\end{aligned}$$

C. Sensitivity computation

For some given wind conditions $\overline{p}$, the sensitivities read as:

$$\nabla_p^2\Phi^\star(\overline{p},\overline{T}) = \left[\nabla_p^2\mathcal{L} + \nabla_{ps}^2\mathcal{L}\frac{\partial s^\star}{\partial p}\right], \quad (8a)$$

$$\nabla_{pT}^2\Phi^\star(\overline{p},\overline{T}) = \left[\nabla_{pT}^2\mathcal{L} + \nabla_{ps}^2\mathcal{L}\frac{\partial s^\star}{\partial T}\right], \quad (8b)$$

$$\nabla_T^2\Phi^\star(\overline{p},\overline{T}) = \left[\nabla_T^2\mathcal{L} + \nabla_{Ts}^2\mathcal{L}\frac{\partial s^\star}{\partial T}\right], \quad (8c)$$

where variable s gathers the primal-dual variables of the problem and all terms are evaluated at $\overline{p},\overline{T}$. If LICQ and SOSC hold at the solution of OCP (2), KKT conditions are satisfied and $\Phi^\star(\overline{p},\overline{T})$ and $s^\star(\overline{p},\overline{T})$ are differentiable in a neighbourhood of $\overline{p},\overline{T}$ [14].

The sensitivities of the parametric primal-dual solution $s^\star(\overline{p},\overline{T})$ are given by:

$$\frac{\partial s^\star}{\partial p} = -\frac{\partial R(s,p,T)}{\partial s}^{-1}\cdot\frac{\partial R(s,p,T)}{\partial p}\bigg|_{s^\star,\overline{p},\overline{T}},$$

$$\frac{\partial s^\star}{\partial T} = -\frac{\partial R(s,p,T)}{\partial s}^{-1}\cdot\frac{\partial R(s,p,T)}{\partial T}\bigg|_{s^\star,\overline{p},\overline{T}},$$

where $R(s,p,T)$ are the primal-dual KKT conditions of OCP (2) [13].

D. Fixed and free orbit times

A performance loss is incurred by assigning the AWE system's orbit times to $\overline{T}$, i.e. the optimal orbit time for the farm average wind condition $\overline{p}$. In order to assess this loss we first observe that, with a fixed orbit time, the variation of performance due to different wind conditions reduces to:

$$\begin{aligned}\Delta\Phi^\star_{\text{fixed}} &= \Delta\Phi^\star(\overline{p}+\Delta p,\overline{T}) \\ &= \nabla_p\Phi^{\star\top}\Delta p + \frac{1}{2}\Delta p^\top\nabla_p^2\Phi^\star\Delta p + \mathcal{O}\left(\|\Delta p\|^3\right)\end{aligned} \tag{9}$$

such that:

$$\mathbb{E}_{\Delta p}\left[\Delta\Phi^\star_{\text{fixed}}\right] \approx \text{Tr}\left[\nabla_p^2\Phi^\star\Sigma_p\right] \tag{10}$$

where Tr denotes the trace of a matrix and Σ_p the diagonal covariance matrix, as Δw_0 and Δz_0 are considered as uncorrelated.

In the free orbit time case the orbit time is optimized with respect to the wind condition variation Δp and the performance variation reads as:

$$\begin{aligned}\Delta\Phi^\star_{\text{free}} = \min_{\Delta T}\ \Delta\Phi^\star(\overline{p}+\Delta p,\overline{T}+\Delta T) \approx \nabla_p\Phi^{\star\top}\Delta p \\ + \min_{\Delta T}\ \frac{1}{2}\begin{bmatrix}\Delta p\\ \Delta T\end{bmatrix}^\top\begin{bmatrix}\nabla_p^2\Phi^\star & \nabla_{pT}^2\Phi^\star\\ \nabla_{Tp}^2\Phi^\star & \nabla_T^2\Phi^\star\end{bmatrix}\begin{bmatrix}\Delta p\\ \Delta T\end{bmatrix}.\end{aligned} \tag{11}$$

The Schur complement of the last term yields the explicit solution:

$$\begin{aligned}\Delta\Phi^\star_{\text{free}} \approx &\nabla_p\Phi^{\star\top}\Delta p \\ &+ \frac{1}{2}\Delta p^\top\left(\nabla_p^2\Phi^\star - \nabla_{pT}^2\Phi^\star\left(\nabla_T^2\Phi^\star\right)^{-1}\nabla_{Tp}^2\Phi^\star\right)\Delta p.\end{aligned} \tag{12}$$

The expected performance then reads as:

$$\begin{aligned}\mathbb{E}_{\Delta p}\left[\Delta\Phi^\star_{\text{free}}\right] \approx &\ \text{Tr}\left[\nabla_p^2\Phi^\star\Sigma_p\right] \\ &- \text{Tr}\left[\nabla_{pT}^2\Phi^\star\left(\nabla_T^2\Phi^\star\right)^{-1}\nabla_{Tp}^2\Phi^\star\Sigma_p\right]\end{aligned} \tag{13}$$

We then observe that the expected performance loss incurred from assigning a fixed orbit time $\Delta T = 0$ instead of using an optimal one as in (12) can be quantified by

$$\begin{aligned}\mathbb{E}_{\Delta p}\left[\Delta\Phi^\star_{\text{fixed}}\right] - \mathbb{E}_{\Delta p}\left[\Delta\Phi^\star_{\text{free}}\right] \approx \\ \text{Tr}\left[\nabla_{pT}^2\Phi^\star\left(\nabla_T^2\Phi^\star\right)^{-1}\nabla_{Tp}^2\Phi^\star\Sigma_p\right] \geq 0.\end{aligned} \tag{14}$$

In the following section, (14) will be used to quantify the performance loss resulting from using phase control in an AWE farm.

III. Numerical results

The investigation on the performance loss is made for pumping and drag mode systems both at small and large scale. The performance losses are quantified at an average roughness of $\overline{z}_0 = 0.15\,\text{m}$ and for the two different average wind farm speeds of $\overline{w}_0 = 6\,\text{m/s}$ and $\overline{w}_0 = 8\,\text{m/s}$. The performance losses are computed for a standard deviation of the base wind speed $\sigma_{\Delta w_0} \in [0, 1.5]\ \text{m/s}$ and for a standard deviation of the roughness $\sigma_{\Delta z_0} \in [0,\ 0.06]\ \text{m}$.

	small-scale		big-scale	
	pump	drag	pump	drag
Area [m^2]	15	20	50	55
wing mass [kg]	100	300	200	1000
tether diameter [m]	0.009	0.013	0.015	0.025
operation altitude [m]	35-160	40-180	60-230	40-200
tether length [m]	240-290	300	420 - 480	300

TABLE I: System specifications for small and big wings

The specifications of the AWE systems considered here are given in Table I. The slightly larger wing area of the drag mode system compensates for the higher component masses, due to the on-board generation. The operation height and the tether length are optimisation results. The wing parameters in Table I are not representing a specific wing, but are chosen as reasonable values.

OCP (2) is discretised using the direct collocation method [13]. The time horizon is split into 40 control intervals, on each of which the state trajectories are represented using a Radau scheme of degree 3. The resulting NLP is solved using Ipopt [15]. The NLP resulting from the discretization of (2) is highly non-convex and very difficult to solve. The problem has been tackled using the approach proposed in [10, 16]. The sensitivity computation detailed in Section II-C uses for the primal-dual KKT conditions R the relaxed KKT conditions deployed in interior-point methods, matching the barrier parameter used by Ipopt.

The optimal trajectory for a pumping mode system at a wind speed of $\overline{w}_0 = 6\text{m/s}$ in x-direction and $\overline{z}_0 = 0.15\,\text{m}$ is shown in the top row in Fig. 3 with a top view on the left and a side view on the right. The number of reel-out cycles have been chosen to three in this analysis. The average power output for this case is 56.74 kW with an optimal orbit time $T = 20.14\,\text{s}$. The resulting power profile has been already shown in Fig. 1b. The optimal trajectory of a drag mode system is roughly a circle operating at similar heights as the pumping mode system, visible in the bottom row of Fig. 3. The average output for this case is 48,4 kW with an orbit time of $T = 6.09\,\text{s}$ and the resulting power profile has been shown in Fig. 1a.

In the following, the performance losses of the drag and pumping mode systems at a mean wind speed of $\overline{w}_0 = 6\,\text{m/s}$ and $\overline{w}_0 = 8\,\text{m/s}$ are presented. The mean roughness factor is kept as $\overline{z}_0 = 0.15\,\text{m}$ for all analysed cases. The difference in performance between the controlled phase and free time case is demonstrated by the relative difference as

$$\Psi = \frac{|\Phi^\star_{\text{free}} - \Phi^\star_{\text{fixed}}|}{\Phi^\star_{\text{free}}}. \tag{15}$$

In order to assess the accuracy of the second-order taylor approximation of $\Phi^\star_{\text{free}}$ proposed here, an example of the difference between the optimal cost $\Phi^\star(\overline{p}+\Delta p,\overline{T}+\Delta T)$ and its second-order approximation is shown in Fig. 4 on the right. On the left the difference of the approximated and the orbit time T solved by the NLP is displayed. This comparison

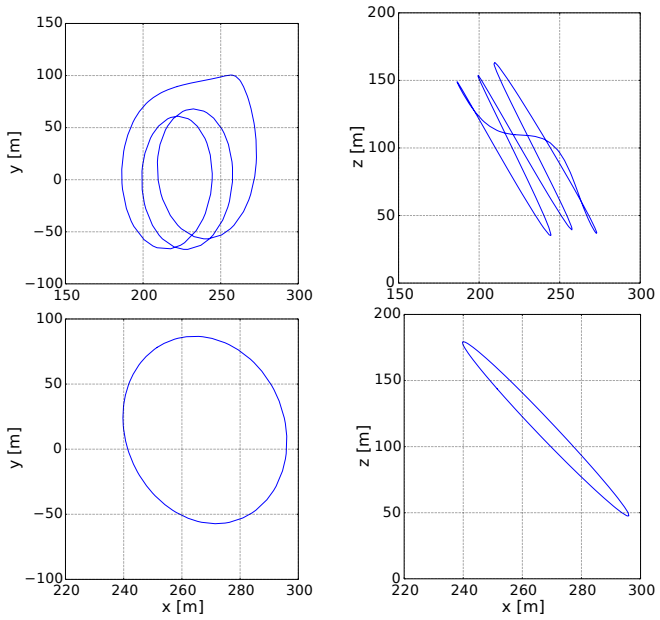

Fig. 3: Optimal trajectory of the small scale pumping mode (top) and the drag mode (bottom) system at $w_0 = 6\,\mathrm{m/s}$ and $z_0 = 0.15\,\mathrm{m}$ with the wind vector pointing in positive x direction. Left: x-y view, right: x-z view

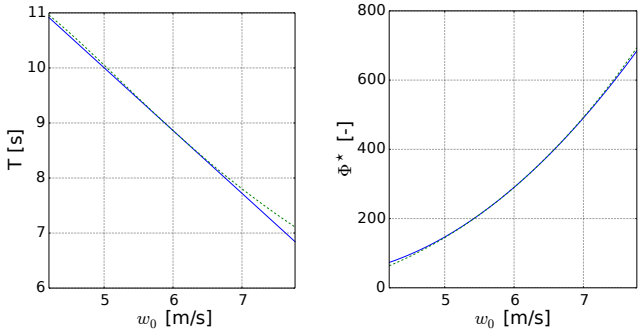

Fig. 4: Comparison of the the approximation and NLP solution for the large-scale drag mode system at $\overline{w}_0 = 6\,\mathrm{m/s}$. Left: difference between the approximated orbit time (blue, solid) and the actual (green, dashed). Right: Difference between the second-order approximated $\Phi^\star_{\mathrm{free}}$ (blue, solid) and the actual performance $\Phi^\star$ (green, dashed).

shows that the proposed approximation is sensible for the reasonably low standard deviations considered throughout the analyses.

In Fig. 5 the relative expected performance differences Ψ are displayed in percent with respect to various standard deviations of Δp. The left plot shows Ψ with respect to a change in the base wind speeds $w_0 = 6\,\mathrm{m/s}$ and $8\,\mathrm{m/s}$. The expected performance loss due to a roughness change Δz_0 from the mean $\overline{z}_0 = 0.15\,\mathrm{m}$ can be seen in the right plot. The top row displays the small-scale and the bottom row the large-scale system.

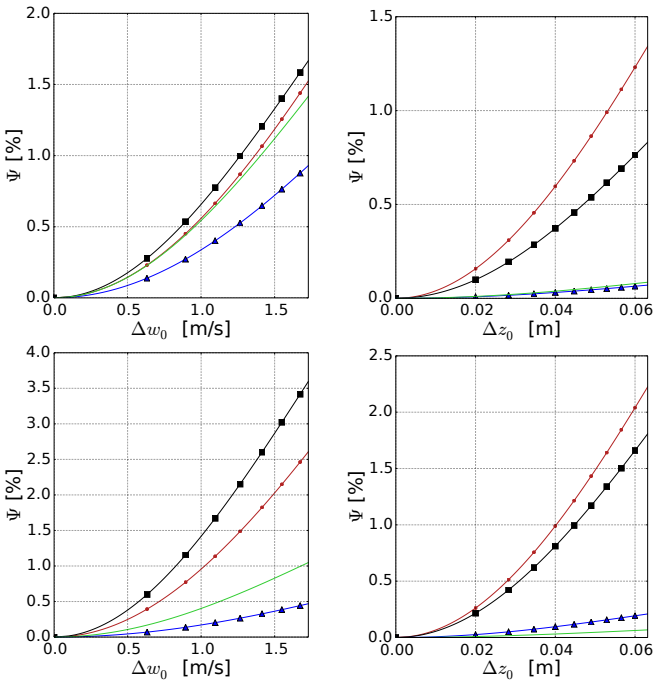

Fig. 5: Expected performance difference Ψ under the variance Δw_0 (left) and under the variance Δz_0 (right). The loss is shown for drag mode system at $\overline{w}_0 = 6\,\mathrm{m/s}$ (black, squares) and $\overline{w}_0 = 8\,\mathrm{m/s}$ (red, dots) as well as for pumping mode systems at $\overline{w}_0 = 6\,\mathrm{m/s}$ (green, solid) and $\overline{w}_0 = 8\,\mathrm{m/s}$ (blue, triangles). Top: small-scale, bottom: large-scale system

For the small-scale system it can be observed that, for drag mode a standard deviation in either the wind speed or roughness factor has a larger effect than in the pumping mode case. In the right plot the pumping mode system shows almost the same relative power difference for $\overline{w}_0 = 6\,\mathrm{m/s}$ and $\overline{w}_0 = 8\,\mathrm{m/s}$. In both cases the relative performance difference is at most 0.1%, so it can be stated that the pumping mode systems are not really affected by a change in roughness. On the other hand, the performance of drag mode systems is clearly sensitive to a deviation in $\overline{z}_0$. Also, the mean base wind in the farm has a clear impact on the performance loss resulting from phase control. The performance loss for roughness changes is more severe at higher mean base winds within a wind farm. This can be seen from the large relative difference in performance for the drag mode system.

For large-scale systems the expected performance loss of the large wings is approximately twice more sensitive to wind variations than for small wings, visible in the bottom row of Fig. 5. This could be due to their higher operation altitude, which means greater winds and thus a higher loss in performance. Otherwise, it shows similar results to the small-scale systems. The drag mode systems show in both plots higher performance losses than the pumping mode. As for the small scale systems, the deviation in $\overline{z}_0$ has a much smaller impact on the pumping mode than on the drag mode.

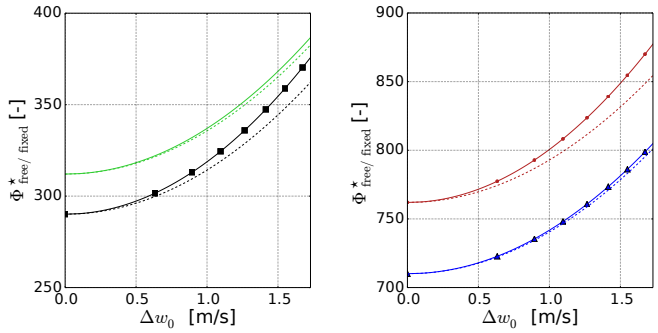

Fig. 6: $\Phi^{\star}_{\text{free}}(\overline{p}+\Delta p, \overline{T}+\Delta T)$ of the large scale systems under the variance Δw_0 shown as solid line and $\Phi^{\star}_{\text{fixed}}(\overline{p}+\Delta p, \overline{T})$ as dashed line for each case respectively. Left: Drag (black, squares) and pumping mode system (green, solid) at $\overline{w}_0 = 6\,\text{m/s}$. Right: Drag (red, dots) and pumping mode system (blue, triangles) at $\overline{w}_0 = 8\,\text{m/s}$.

The expected performance $\Phi^{\star}_{\text{fixed}}$ and $\Phi^{\star}_{\text{free}}$ for the large scale systems is displayed in Fig. 6. The greater performance for a free orbit time is clearly visible, especially for the drag mode system. Note, that as stated earlier, the performance index is essentially yielding the power generation. Hence, the performance represents the power generation in kW.

IV. Conclusion

The AWE industry is considering tackling the problem of power variation of AWE systems via power averaging over AWE farms. A technologically simple deployment of this approach requires fixing the orbit times of the AWE systems in the AWE farm, such that all systems in the farm follow the same trajectory and orbit time. The selected orbit time would be optimised with respect to the average wind speed in the AWE farm. This, however, prevents the individual AWE systems from exploiting their individual wind conditions to the fullest, and therefore leads to a loss of performance. This paper quantifies this loss of performance. It is computed by comparing the expected performance of an AWE farm operating using fixed orbit time vs. orbit times optimized for the individual wind conditions. The study investigates both small and large-scale systems for both the drag and pumping mode, and considers variations of the wind speed and wind shear in the AWE farm.

For all analysed cases, assigning a fixed orbit time to all AWE systems in the wind farm, according to the average wind conditions present in the farm, has a limited impact on the performance. The performance loss does not exceed 4% in all cases. The pumping mode is less sensitive to fixing the orbit times than the drag mode, indeed, in the pumping mode case, the performance loss does not exceed 1.4%.

According to these results, power averaging via a simple phase shift and fixing of the orbit time appears a reasonable approach to mitigate the power variations in AWE farms. With respect to future requirements of power averaging in AWE farms, this quantification of performance loss gives an indication of the economic viability of the phase-shifting control approach. We need to report here, however, that these observations appear to be influenced by the wing aerodynamics. While a reasonable choice of aerodynamic model was made in this paper, the performance loss obtained for a wider range of models ought to be investigated to further explore this question.

Further work will investigate the effect the wind variations at the level of the individual AWE systems with fixed orbit times will have on the overall AWE farm power.

Acknowledgment

This project has received funding from the European Union's Horizon 2020 research and innovation programme under the Marie Skłodowska-Curie grant agreement No 642682. Disclaimer: This document reflects only the author's view. The Commission is not responsible for any use that may be made of the information it contains.

References

[1] A. Cherubini, A. Papini, R. Vertechy, and M. Fontana, "Airborne wind energy systems: A review of the technologies," *Renewable and Sustainable Energy Reviews*, vol. 51, pp. 1461 – 1476, 2015.

[2] M. Diehl, *Model-Based Efficiency Analysis of Wind Power Conversion by a Pumping Kite Power System*, pp. 3–22. Berlin, Heidelberg: Springer Berlin Heidelberg, 2013.

[3] R. H. Luchsinger, *Pumping Cycle Kite Power*, pp. 47–64. Berlin, Heidelberg: Springer Berlin Heidelberg, 2013.

[4] U. Fechner and R. Schmehl, *Model-Based Efficiency Analysis of Wind Power Conversion by a Pumping Kite Power System*, pp. 249–269. Berlin, Heidelberg: Springer Berlin Heidelberg, 2013.

[5] "www.ampyxpower.com," 2017.

[6] T. Ackermann, *Wind power in power systems*. Wiley, 2012.

[7] IRENA, *Scaling up Variable Renewable Power: The Role of Grid Codes*, 2016.

[8] J. Bossuyt, M. Howland, C. Meneveau, and J. Meyers, "Measurement of unsteady loading and power output variability in a micro wind farm model in a wind tunnel," vol. 58, 12 2016.

[9] S. Costello, G. Francois, and D. Bonvin, "Real-time optimization for kites," *IFAC Proceedings Volumes (IFAC-PapersOnline)*, vol. 5, pp. 64–69, 2013.

[10] G. Horn, S. Gros, and M. Diehl, *Numerical Trajectory Optimization for Airborne Wind Energy Systems Described by High Fidelity Aircraft Models*, pp. 205–218. Berlin, Heidelberg: Springer Berlin Heidelberg, 2013.

[11] L. Landberg, *Meteorology for wind energy: an introduction*. Wiley, 1 ed., 2016.

[12] S. Gros and M. Diehl, *Modeling of Airborne Wind Energy Systems in Natural Coordinates*, pp. 181–203. Berlin, Heidelberg: Springer Berlin Heidelberg, 2013.

[13] L. Biegler, *Nonlinear Programming*. Society for Industrial and Applied Mathematics, 2010.

[14] J. Nocedal and S. Wright, *Numerical Optimization*. Springer, 2006.

[15] A. Wächter and L. T. Biegler, "On the implementation of an interior-point filter line-search algorithm for large-scale nonlinear programming," *Mathematical Programming*, vol. 106, no. 1, pp. 25–57, 2006.

[16] S. Gros, M. Zanon, and M. Diehl, "A relaxation strategy for the optimization of airborne wind energy systems," in *2013 European Control Conference (ECC)*, pp. 1011–1016, July 2013.

[17] U. Ahrens, M. Diehl, and R. Schmehl, *Airborne Wind Energy*. Springer, 2011.

[18] M. L. Loyd, "Crosswind kite power," *Journal of Energy*, vol. 4, pp. 106–111, June 1980.